Chem Biol Drug Des 2014; **83:** 401–410

Research Article

Beyond Topoisomerase Inhibition: Antitumor 1,4-Naphthoquinones as Potential Inhibitors of Human Monoamine Oxidase

Eduardo Coelho-Cerqueira[1], Paulo A. Netz[2], Vanessa P. do Canto[2], Angelo C. Pinto[3] and Cristian Follmer[1,*]

[1]Department of Physical Chemistry, Institute of Chemistry, Federal University of Rio de Janeiro, Rio de Janeiro 21941-909, Brazil
[2]Institute of Chemistry, Federal University of Rio Grande do Sul, Porto Alegre, 91501-970, Brazil
[3]Department of Organic Chemistry, Institute of Chemistry, Federal University of Rio de Janeiro, Rio de Janeiro 21941-909, Brazil
**Corresponding author: Cristian Follmer, follmer@iq.ufrj.br*

Monoamine oxidase (MAO) action has been involved in the regulation of neurotransmitters levels, cell signaling, cellular growth, and differentiation as well as in the balance of the intracellular polyamine levels. Although so far obscure, MAO inhibitors are believed to have some effect on tumors progression. 1,4-naphthoquinone (1,4-NQ) has been pointed out as a potential pharmacophore for inhibition of both MAO and DNA topoisomerase activities, this latter associated with antitumor activity. Herein, we demonstrated that certain antitumor 1,4-NQs, including spermidine-1,4-NQ, lapachol, and *nor*-lapachol display inhibitory activity on human MAO-A and MAO-B. Kinetic studies indicated that these compounds are reversible and competitive MAO inhibitors, being the enzyme selectivity greatly affected by substitutions on 1,4-NQ ring. Molecular docking studies suggested that the most potent MAO inhibitors are capable to bind to the MAO active site in close proximity of flavin moiety. Furthermore, ability to inhibit both MAO-A and MAO-B can be potentialized by the formation of hydrogen bonds between these compounds and FAD and/or the residues in the active site. Although spermidine-1,4-NQs exhibit antitumor action primarily by inhibiting topoisomerase via DNA intercalation, our findings suggest that their effect on MAO activity should be taken into account when their application in cancer therapy is considered.

Key words: cancer, flavin, lapachol, monoamine oxidase, naphthoquinones, spermidine

Received 25 July 2013, revised 24 September 2013 and accepted for publication 22 October 2013

Monoamine oxidases (MAO) [amine: oxygen oxidoreductase (deamination) (flavin containing) EC 1.4.3.4.] catalyze the major route of inactivation of neurotransmitters, such as dopamine, epinephrine, and norepinephrine by promoting the oxidation of amines to the corresponding aldehydes, with the generation of hydrogen peroxide (1). Two MAO isoforms have been identified, MAO-A and MAO-B, which have a sequence identity of approximately 72% and differ from each other in relation to substrate and inhibitor specificity. MAO-A acts preferentially on 5-hydroxytryptamine, whereas MAO-B is more active on arylalkylamines such as benzylamine, preventing exogenous amines from acting as false neurotransmitters (1,2). Additionally, MAO-B participates in the oxidative metabolism of exogenous amines such as the neurotoxin 1-methyl-4-phenyl-1,2,3,6-tetrahydropyridine (MPTP), which is converted to MPP^+ that causes Parkinson-like symptoms in human and other primates (2,3).

The activity of both MAO isoforms is augmented with aging, leading to an increase in the side product hydrogen peroxide, accompanied by a reduction in the levels of certain neurotransmitters (1,4). While the level of MAO-B increases 4- to 5-fold during aging and was associated with neurodegenerative disorders (4), MAO-A level was significantly enhanced in hearts of aged rats and was associated with cardiac cellular degeneration (5). In addition, MAO activity is enhanced in certain tumor cells (6,7). In this context, extensive efforts have been made to develop efficient and safe MAO inhibitors, notably for Alzheimer disease and Parkinson's disease therapy (inhibition of MAO-B isoform) and for depression illness (inhibition of MAO-A) (1).

Several evidences have pointed out that MAO is a promising target for cancer therapy: (i) A significant and selective MAO-B activity is enhanced in malignant tumors in central nervous system (6,7). In astrocytomas, the degree of tumor malignancy has been positively correlated with the amine oxidase activity (8). (ii) Isatin, an endogenous MAO-B inhibitor, is capable to induce apoptosis or necrosis in human neuroblastoma cells (9) due to an intracellular accumulation of monoamines and increase in the production of reactive oxygen species (ROS) (10). (iii) In prostate cancer, MAO-A inhibitors such as clorgyline might restore

 doi: 10.1111/cbdd.12255

differentiation and hence reverse the aggressive characteristic of high-grade cancer (11). Therefore, MAO-A and MAO-B might represent an important target for new therapeutic strategies for different types of tumors.

Recently, it has been shown that 1,4-naphthoquinone (1,4-NQ) is a potential scaffold for designing reversible MAO inhibitors in which the selectivity may be easily altered by changes in the substituents on the naphthoquinone ring (12,13). Furthermore, certain 1,4-NQs display inhibitory properties on important biological targets, including DNA topoisomerase activity (14), amyloid β-peptide and α-synuclein fibrillization (15,16), and Hsp90 activity (17). Naphthoquinones such as lapachol (2-hydroxy-3-prenyl-1,4-naphthoquinone) and *nor*-lapachol [2-hydroxy-3-(2-methylpropenyl)-1,4-naphthoquinone] were described to have antitumor action against several cancer cells (14,18). Recently, the antitumor activity of 2-spermidine-3-R-1,4-naphthoquinones was demonstrated for cancer cell lines such as human promyelocytic leukemia, lung cancer, Burkitt lymphoma, and mouse breast tumor (18). Studies of the antitumor properties and mechanisms of action of quinone derivatives have shown that they can act as topoisomerase inhibitors via DNA intercalation (14). These molecules display a 1,4-NQ scaffold, which is associated with both DNA topoisomerase and MAO inhibition, conjugated with a polyamine such as spermidine, which is substrate for MAO and other amine oxidases. Interestingly, the level of polyamines such as N1-(3-aminopropyl)-1,4-butanediamine (spermidine, **d**) is increased in tumors as compared to normal tissues, and their intracellular accumulation can induce apoptosis in different cell lines (19,20). Analogs of natural polyamines might compete with naturally occurring polyamines for critical cellular binding sites (18). In this context, the conjugation of spermidine analogs with a cytotoxic compound was used to increase in their chemotherapeutic activity by either facilitating their entry into tumor cells (via polyamine uptake systems) or increasing their selectivity to DNA (18).

In this work, we synthesized and evaluated the inhibitory activity on human MAO-A and MAO-B of antitumor polyamine-1,4-NQs containing a spermidine analog (benzyl-spermidine) conjugated to 1,4-NQ, lapachol, or *nor*-lapachol. The molecular mechanisms lying behind the inhibition of MAO isoforms were investigated using molecular modeling tools. These antitumor compounds inhibited MAO isoforms by a competitive mechanism in which the enzyme selectivity was greatly influenced by substitutions on 1,4-NQ ring. In addition, molecular docking results suggested that spermidine-1,4-NQs that act as potent inhibitors of MAO are capable of binding to the catalytic site of MAO in close proximity of flavin moiety. Although previous studies have already pointed out that 1,4-NQ represents an important scaffold for the development of both MAO and DNA topoisomerase inhibitors, it was the first time that 1,4-NQs with potential antitumor activity against several cancer cell lines were evaluated in respect to inhibition of MAO activity. In light of these findings, we have discussed the role of MAO activity in cancer growth as well as the importance of MAO inhibition in antitumor therapies.

Experimental

Synthesis of spermidine-1,4-NQs

Spermidine-1,4-NQs $\mathbf{a_1}$, $\mathbf{b_1}$, and $\mathbf{c_1}$ were synthesized and characterized as described by Cunha *et al.* (21). The synthesis steps are indicated in Figure 1, in which one can verify that $\mathbf{a_1}$ and $\mathbf{a_2}$ compounds are structurally related to lapachol (**a**), whereas the $\mathbf{c_1}$ and $\mathbf{c_2}$ compounds are related to *nor*-lapachol (**c**). The $\mathbf{b_1}$ and $\mathbf{b_2}$ compounds are related to lawsone (**b**), that is, they display a hydrogen at the 3-position in the 1,4-NQ ring. The steps of the synthesis were as follows: (i) the methylation of lapachol (**a**) and *nor*-lapachol (**c**) with dimethylsulphate in acetone and potassium carbonate to yield $\mathbf{a_0}$ and $\mathbf{c_0}$, and synthesis of methoxylawsone ($\mathbf{b_0}$) from the sodium salt of 1,2-naphthoquinone-4-sulfonic acid; (ii) preparation of the protected derivative of spermidine $\mathbf{d_0}$ in a four-step synthesis; (iii) nucleophilic displacement of the methoxyquinones $\mathbf{a_0}$, $\mathbf{b_0}$, and $\mathbf{c_0}$ with compound $\mathbf{d_0}$ (Figure 1). To remove the protecting group BOC, a solution of TFA (0.20 ml; 2.6 mmol) in CH_2Cl_2 (5 mL) was slowly added to a solution of $\mathbf{b_1}$ (62.7 mg; 0.13 mmol) in methanol (20 mL) at 0 °C. After 10 min, the reaction was taken to room temperature and kept under stirring for 4 h until total consumption of the starting material. The solvent was removed under reduced pressure; addition of 10% $KHCO_3$ (10 mL) was followed by extraction with CH_2Cl_2 (3 × 20 mL). The organic phase was dried with anhydrous Na_2SO_4 and concentrated under reduced pressure to give the free amine $\mathbf{b_2}$ (50.3 mg, 99%), as a red oil that was purified by flash chromatography (ethyl acetate/methanol, 6:4). [R*f* = 0.2 (CH_2Cl_2/methanol/triethylamine 10:89:1)]. Infrared (film) ν_{max} (cm^{-1}): 3353, 3063, 3003, 2973, 2805, 1708, 1606,1509, 721, 698. ^{1}H NMR (200 MHz, $CDCl_3$): δ 1.59 (m, 6H), 2.42 (t, J = 6.2 Hz, 2H), 2.50 (t, J = 6.2 Hz, 2H), 3.11 (m, 4H), 3.53 (s, 2H), 5.28 (brs, 1H), 5.68 (s, 1H), 5.99 (s, 1H), 7.30 (m, 5H), 7.61 (brt, J = 7.5, 1H), 7.73 (brt, J = 7.5, 1H), 8.05 (d, J = 7.5, 1H) and 8.11 (d, J = 7.5 Hz, 1H). ^{13}C NMR (50 MHz, $CDCl_3$): δ 24.6, 25.9, 26.1, 28.5, 34.0, 42.4, 52.4, 53.1, 58.9, 126.2, 129.0, 131.9, 134.7, 139.2, 149.2, 183.1, 184.3. MS found: 392.2359 [$\mathbf{b_2}$+1]+; calculated for [$C_{24}H_{29}N_3O_2$]+ 392.2338.

Similar procedure was followed for the syntheses of compounds $\mathbf{a_2}$ and $\mathbf{c_2}$. Product $\mathbf{a_2}$ was purified as above using ethyl acetate/methanol 6:4 as eluent and obtained as brown reddish oil (57.9 mg, 97%). [R*f* = 0.2 (CH_2Cl/methanol/triethylamine 10:89:1)]. Infrared (film) ν_{max} (cm^{-1}): 3347, 3063, 3027, 2930, 2863, 1712, 1602, 1570, 1515, 721, 698. ^{1}H NMR (200 MHz, $CDCl_3$): δ 1.60 (m, 4H), 1.68 (brt, 3H), 2.42 (t, J = 6.4 Hz,2H), 2.48 (t, J = 6.4 Hz, 2H), 3.15 (m, 2H), 3.40 (m, 4H), 3.52 (s, 2H), 5.06 (m, 1H), 5.25 (m, 1H), 5.67 (m, 1H), 7.56 (brt, J = 7.5 Hz, 1H),

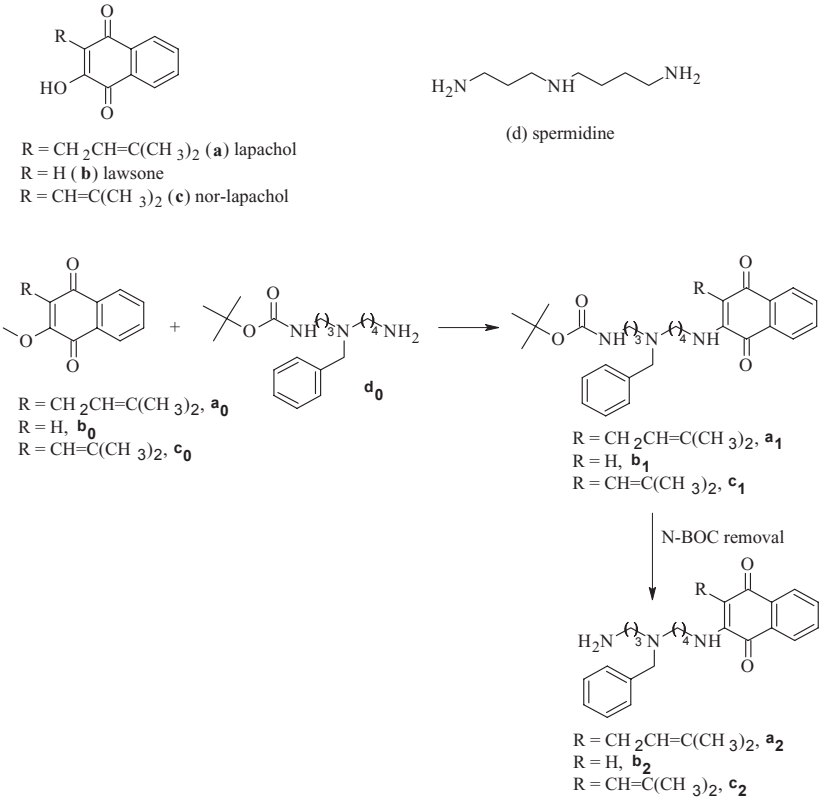

Figure 1: Steps of the synthesis of spermidine-1,4-NQs.

7.67 (brt, J = 7.5 Hz, 1H), 7.99 (dd, J = 7.5 Hz, 1H), 8.09 (dd, J = 7.5 Hz, 1H). ^{13}C NMR (50 MHz, $CDCl_3$): δ 18.2, 23.8, 24.3, 25.8, 26.6, 29.2, 39.3, 45.0, 52.7, 53.4, 58.9, 115.4, 123.2, 126.2, 127.2, 128.7, 130.5, 132.0, 133.6, 134.4, 139.4, 145.7, 183.1. MS found: 460.2943 [**a$_2$**+1]+; calculated for [$C_{29}H_{37}N_3O_2$]+ 460.2964. Product **c$_2$** was purified as above using ethyl acetate/methanol, 6:4 as eluent as red oil (55.5 mg, 96%) [R*f* = 0.2 (CH_2Cl_2/methanol/triethylamine 10:89:1)]. Infrared (film) ν_{max} (cm^{-1}): 3354–3347, 3063, 3027, 2972, 2806, 1712, 1602, 1515, 1170, 721, 698. ^{1}H NMR (200 MHz, $CDCl_3$): δ 1.46 (m, 5H); 1,61 (m, 4H); 1,92 (s, 3H); 2,42 (m, 4H, J = 6.3); 2.61 (t, 2H, J = 6.3 Hz); 4,60 (t, 2H, J = 6.3); 3.50 (s, 2H); 5.34 (br s, H); 5.91 (t, 1H); 6.10 (s, 1H); 7,54 (m, 5H); 7,63 (dt, 2H, J = 7.5); 8,06 (dd, 2H, J = 7.5). ^{13}C NMR (50 MHz, CDCl3): δ 20.3, 24.5, 25.6, 26.9, 28.0, 39.9, 44.4, 39.9, 53.5, 59.0, 113.5, 118.0, 126.1, 126.5, 127.3, 128.5, 129.1, 130.6, 132.0, 133.8, 134.7, 135.3, 138.7, 139.5, 144.8, 183.1, 183.5. MS found: 446.2837 [**c$_2$**+1]+; calculated for [$C_{28}H_{35}N_3O_2$]+ 446.2807.

MAO assay

Microsomes from baculovirus-infected insect cells that express recombinant human MAO-A and MAO-B were purchased from Sigma-Aldrich Co (St Louis, MO, USA). The activities of MAO-A and MAO-B were evaluated by a fluorometric assay that measures the amount of resorufin produced from Amplex Red® (AR) (Life Technologies, Carlsbad, CA, USA) in the presence of hydrogen peroxide (generated by MAO activity) and horseradish peroxidase (HRP) (22). These assays were carried out in a 96-well microplate. The fluorescence intensity was measured by a fluorescence microplate reader in a Cary Eclipse Fluorimeter (Agilent Technologies, Santa Clara, CA, USA) with excitation at 571 nm and emission at 585 nm. The effect of the inhibitors on the fluorescence emission of resorufin at 585 nm was previously evaluated, and a correction was performed when necessary. The reaction mixture (final volume of 200 μL) contained 5 μg/mL MAO-A or MAO-B in a 50 mM sodium phosphate buffer pH 7.4, 1 mM p-tyramine (substrate for MAO-A) or 1 mM benzylamine (substrate for MAO-B), 1 U/mL HRP, and 200 μM AR. This mixture was incubated, in the presence or absence of the inhibitors, at 37 °C for 45 min using a Thermomixer equipment (Eppendorf, Hamburg, Germany). The enzyme plus the inhibitors were incubated at 37 °C for 20 min prior to the addition of the substrates, HRP and AR. The inhibitors were dissolved in 100% DMSO, and equivalent concentrations of DMSO alone (1–2%) were used as controls. Clorgyline (MAO-A inhibitor) or pargyline (MAO-B inhibitor) at 5 μM concentration was used as positive control for inhibition. To verify whether the inhibitors affect the enzymatic assay by either inhibiting the AR oxidation by HRP or by scavenging the hydrogen peroxide that was generated, hydrogen peroxide was preincubated in the presence or absence of the inhibitors, and 1 U/mL HRP, 1 mM substrate, and 200 μM AR were

added to the reaction mixture. This mixture was incubated at 37 °C for 45 min, and the resorufin content was determined by fluorescence, as described above. The enzymatic activity was expressed as nanomols of hydrogen peroxide produced per milligram of enzyme per minute at pH 7.4 and 37 °C. We varied the amount of hydrogen peroxide used (0.4–3.2 nmols) to create a calibration curve.

Kinetic parameters

The enzymatic kinetic parameters Michaelis–Menten constant (Km) and maximum reaction rate (V_{max}) were determined by nonlinear fitting using the NLfit tool and the *Hill* function in OriginLab 8.0 software (OriginLab Co, Northampton, MA, USA). The inhibitory constant *Ki* was determined by the relation: Km'/Km = 1 + [I]/*Ki*, where Km' and Km are the Michaelis–Menten constant in the presence and the absence of inhibitor, respectively, and [I] is the concentration of the inhibitor. The mechanism of inhibition was confirmed by the Lineweaver–Burk curves (double reciprocal plot) by plotting the inverse of initial velocity (1/V) as a function of the inverse of the substrate concentration (1/S) (23).

Molecular modeling: ligand and receptor building

The structures of menadione, lapachol, *nor*-lapachol, and the spermidine-1,4-naphthoquinones (**a_2**, **b_2**, and **c_2**) were built with GaussView (24) and optimized with RHF/6-31G (d,p) using GAUSSIAN 09 (25). Considering that the spermidine derivatives have many potential protonation sites, the pKA of each amine group and the protonation pattern at physiological conditions were calculated with MarvinSketch [Marvin 5.12.3 (Evaluation Mode), 2013, ChemAxon (www.chemaxon.com/marvin/sketch/index.php)], and the resulting protonated structures were re-optimized with AM1 method using GAUSSIAN 09. The final structures were converted to the *mol2* format. Using AutoDock Tools (26), the non-polar hydrogen atoms were merged to the heavy atoms. Gasteiger–Marsili partial charges are assigned as described (27). The final structures were written as *pdbqt* files for further use in AutoDock (28,29) and AutoDockVina (30) dockings.

The MAO-A receptor structure was built as a modification of a structure obtained from the Protein Data Bank (PDB: 2Z5X) (31). This structure includes a monomeric form of MAO-A interacting non-covalently with FAD and the reversible inhibitor harmine (HRM, 7-methoxy-1-methyl-9H-beta-carboline). The co-ordinates of harmine and crystallization water molecules were deleted, and only the co-ordinates of the protein and FAD were used as starting point for the construction of the receptor structures, as detailed below. The MAO-B receptor structure was built as a modification of the structure obtained from the Protein Data Bank (PDB: 2VRL) (32). This structure contains a dimeric form of the human MAO-B, with each chain containing FAD and benzylhydrazine. For docking purposes, only the co-ordinates of chain A and FAD were considered as starting point for the construction of the receptor structure.

Molecular modeling: grid and docking

The spermidine derivatives are bulky ligands and are able to fit only roughly in the binding site as displayed in the original PDB receptor structures. The structures obtained from the Protein Data Bank depend strongly on the experimental conditions at which they were determined. It is reasonable, thus, to relax the receptor's structures before the docking and to obtain an adequate ensemble of conformations, where the receptor is able, in principle, to interact with ligands of several sizes. Therefore, we choose an ensemble docking method similar to the Relaxed Complex Scheme (33–35) in order to sample adequate conformations, suitable to interact with those ligands. We carried out 50 ns long molecular dynamics simulations of the Holo form [bound with FAD and menadione (13)] of MAO-A and MAO-B. At each 5 nseconds, snapshots were extracted and the protein and FAD co-ordinates used as receptor for docking purposes. The best scores for each ligand in each snapshot were recorded, and we could therefore obtain a dynamical evaluation of the docking poses, which can be correlated with receptor's structural changes. The molecular dynamics (MD) simulations for the generation of the trajectory were carried out with the GROMACS package (36) using GROMOS 53A6 force field (37), in the NPT ensemble, using PME electrostatic calculations. Explicit SPC (simple point charge) water molecules located in a simulation box was used. Snapshots were generated using programs into Gromacs package, and the structures of the receptors were prepared using AutoDock tools. The receptor structures in each snapshot were fitted to the initial structure, using the FAD moiety as reference. The ensemble docking was carried out, with help of home-made scripts, with AutoDock Vina, using a grid of 23 × 23 × 23 Angstroms centered in the active site. All dockings using AutoDock Vina were carried out in triplicate.

For dockings using the AutoDock program, the receptor structures were chosen according to AutoDock Vina results, selecting the snapshots that provided the major discrimination between ligands, 30 nseconds for MAO-A and 20 nseconds for MAO-B. A grid box was built with a resolution of 0.375 Angstrons and 61 × 61 × 61 points and constituted a region surrounding the interaction site close to FAD, inside the enzymes. The docking was carried out by AutoDock 4.2 (38) with a Lamarckian Algorithm (Genetic Algorithm combined with a local search). The following parameters were chosen: 100 GA runs, population size of 50, number of evaluations 50 000 000, number of generations 27 000, maximum number of top individuals of 1, gene mutation rate of 0.02, and a crossover rate of

0.8. The AutoDock 4.2 default values were used for the remaining docking parameters, except for the step-size parameters that were chosen to be 0.2 Å (translation) and 5.0 degrees (quaternion and torsion). The docked conformations were clustered according to their geometrical similarity (rms of 2.0 Å) and docked energy. The interactions between the ligand and protein residues were analyzed with AutoDockTools (26).

Results and Discussion

Kinetic features of MAO inhibition

By using a very sensitive fluorescent method to measure MAO activity, the inhibitory effect of a series of antitumor 1,4-NQs (spermidine-1,4-NQs, lapachol, and *nor*-lapachol) on MAO activity was investigated. It is important to note that these 1,4-NQs did not interfere in the reaction of formation of resorufin from AR in the presence of hydrogen peroxide and HRP, similarly to described for 1,4-NQ and menadione (13). In addition, these compounds neither interfered in resorufin fluorescence (e.g., by quenching the fluorescence) nor act as scavenger of hydrogen peroxide that was produced during the reaction (data not shown).

Table 1 shows the inhibitory constant *Ki* and the enzyme selectivity ($Ki^{MAO\text{-}A}/Ki^{MAO\text{-}B}$) for MAO inhibition by spermidine-1,4-NQs (**a_2**, **b_2**, and **c_2**), lapachol, and *nor*-lapachol. The mechanisms of inhibition as well as the *Ki* values were determined through a nonlinear regression of Michaelis–Menten curves as illustrated in Figure 2. Both lapachol and *nor*-lapachol were less effective MAO inhibitors than either 1,4-NQ or menadione, this latter being the most potent and selective 1,4-NQ described so far with *Ki* = 0.4 μM and 65-fold selectivity for MAO-B (13). Lapachol inhibited MAO-B with a *Ki* value of 59 μM, but it did not have any effect on MAO-A at a concentration of 100 μM. On the other hand, *nor*-lapachol inhibited both isoforms with similar *Ki* values: 35 and 18 μM for MAO-A and MAO-B, respectively. Therefore, *nor*-lapachol, with a poor selectivity for MAO-B, was less potent and selective than menadione or 1,4-NQ for this isoform.

Table 1: Kinetic data of the inhibition of MAO by 1,4-NQs. Results are shown as mean ± standard deviation for three experiments.*Ref (7.); # no inhibition at up 100 μM

	Inhibitory constant *Ki* (μM)		
	MAO-A	MAO-B	$Ki^{MAO\text{-}A}/Ki^{MAO\text{-}B}$
1,4-NQ*	7.7	1.5	5.1
Menadione*	26	0.4	65
Lapachol#	–	59 ± 9	–
Nor-lapachol	35 ± 6	18 ± 8	1.9
a_2	22 ± 3	40 ± 6	0.5
b_2	28 ± 5	12 ± 3	2.3
c_2	63 ± 12	58 ± 7	1.1

Analyzing the data in Table 1, one can observe that all spermidine-1,4-NQs were capable to inhibit MAO isoforms with a poor selectivity, exhibiting *Ki* values in the range of 12–63 μM. The most potent inhibitor of MAO-B was **b_2** with a *Ki* = 12 μM and a 2-fold selectivity for this isoform. For MAO-A, **a_2** exhibited the lowest *Ki* value (22 μM), being the most selective among the spermidine-1,4-NQs. The effect of the inhibitors (50 μM) on the parameters K_m and V_{max} for MAO-A and MAO-B is shown in Table 2. The K_m values for MAO-A and MAO-B in the absence of the inhibitors were 370 ± 68 μM (V_{max} = 36 ± 4 nmol/min.mg) and 497 ± 203 μM (V_{max} = 19 ± 4 nmol/min.mg), respectively. An increasing of K_m without changes in V_{max} was observed for all inhibitors, which indicates a competitive mechanism. The most remarkable alteration for K_m was observed for the compounds exhibiting the lowest *Ki* values, that is, **a_2** for MAO-A and *nor*-lapachol and **b_2** for MAO-B. The minor MAO inhibitors, lapachol, **a_2**, and **c_2** for MAO-B and **c_2** for MAO-A, did not produce significant effects on K_m at a concentration of 50 μM (Table 2). Collectively, our data suggest that antitumor 1,4-NQs are competitive MAO inhibitors in which the enzyme selectivity is remarkably dependent on the substitutions on 1,4-NQ ring. While 1,4-NQ inhibits MAO-A by a non-competitive mechanism (13), its derivatives with substitutions on either 2- or 3-position of 1,4-NQ ring behave exclusively as competitive inhibitors. Molecular modeling data suggest that 1,4-NQ interacts with MAO-A residues located in the inner portion of the enzyme instead of those in the catalytic site, which may explain the observed non-competitive mechanism (13).

Two important features must be taken into account for the development of new MAO inhibitors: the reversibility and the selectivity. The reversibility and non-selectivity might represent, in certain cases, an advantage in comparison with irreversible and selective inhibitors, even though reversible inhibitors are often less potent than irreversible inhibitors. Similar to other 1,4-NQs, spermidine-1,4-NQs, lapachol, and *nor*-lapachol behave as reversible MAO inhibitors. The reversibility is an important feature for inhibitors targeting MAO-A. As tyramine is metabolized by MAO-A in the intestine, the irreversible inhibitors of MAO-A might produce a side-effect known as 'cheese reaction' that is characterized by an elevation of the sympathetic cardiovascular activity via the release of norepinephrine (39). Because the intestine contains a low MAO-B content, the administration of MAO-B inhibitors does not promote the cheese reaction unless the inhibitor is administered in a dose high enough to inhibit MAO-A. Furthermore, spermidine-1,4-NQs and *nor*-lapachol were in general poorly selective inhibitors. In contrast with menadione that exhibits 65-fold selectivity to MAO-B, the most selective inhibitors of MAO-B among the antitumor 1,4-NQs, i.e., *nor*-lapachol and **b_2**, exhibited ~ 2-fold selectivity for this isoform. Similar selectivity for MAO-A was observed for **a_2**, the most potent inhibitor among antitumor 1,4-NQs

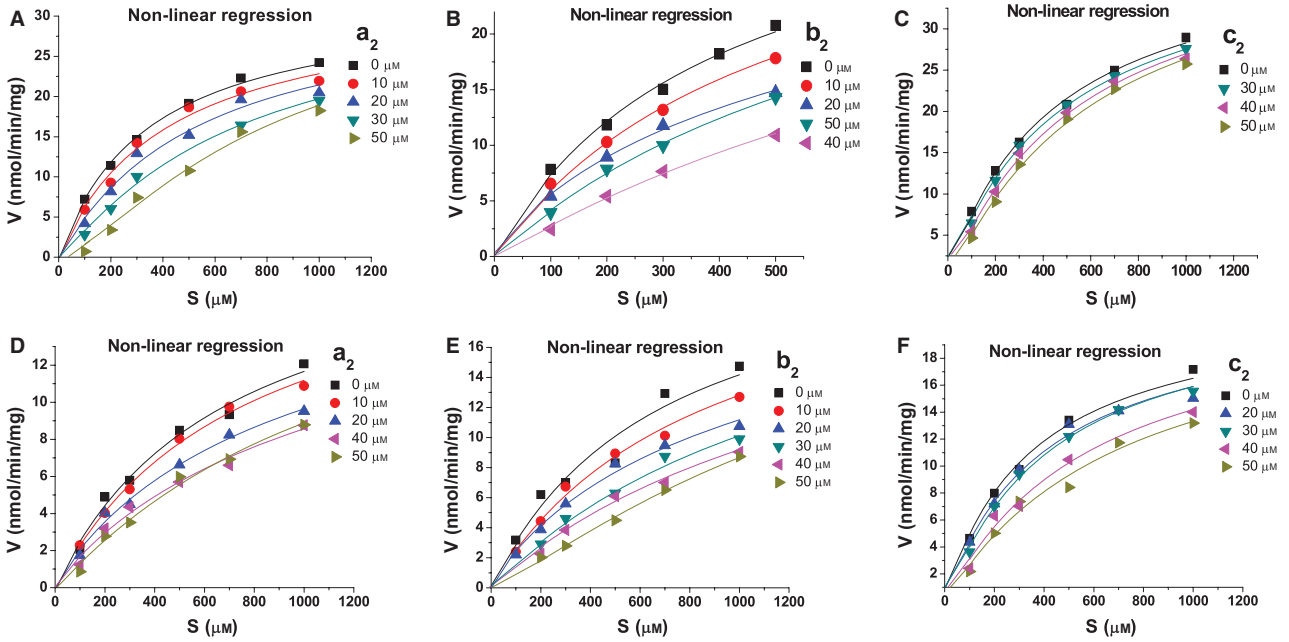

Figure 2: Kinetics of the inhibition of human MAO by antitumor spermidine-1,4-NQs. The effect of varying concentrations of the inhibitors **a_2**, **b_2**, and **c_2** on MAO-A (A, B, and C, respectively) and on MAO-B (D, E, and F, respectively) was analyzed by nonlinear fitting. Benzylamine and *p*-tyramine were used as substrates for MAO-B and MAO-A, respectively.

Table 2: Kinetic parameters (K_m and V_{max}) for MAO-A and MAO-B in the presence of 50 μM of lapachol, *nor*-lapachol, or spermidine-1,4-NQs. Results are shown as mean ± standard deviation for three experiments. *Mean ± SD for six experiments

	MAO-A		MAO-B	
	K_m (μM)	V_{max} (nmol/min. mg)	K_m (μM)	V_{max} (nmol.min. mg)
Control*	370 ± 68	36 ± 4	497 ± 203	19 ± 4
Lapachol	–	–	749 ± 107	13 ± 2
Nor-lapachol	759 ± 54	35 ± 1	1208 ± 162	17 ± 2
a_2	789 ± 64	32 ± 2	650 ± 127	20 ± 1
b_2	758 ± 92	36 ± 2	1587 ± 298	24 ± 2
c_2	490 ± 60	41 ± 1	587 ± 63	22 ± 1

(Table 1). The non-selectivity in the MAO inhibition is an important feature when the goal is the oxidation of amines that are substrates of both MAO isoforms. For instance, the administration of non-selective MAO inhibitors might result in an increase in dopamine level that is not observed for many selective inhibitors (40). Dopamine is metabolized by both MAO isoforms: by MAO-A intraneuronally and by MAO-A/MAO-B in glial and astrocyte cells (1). Therefore, the selective inhibition of an isoform can be counterbalanced by an increase in the activity of the other isoform. In this context, the poor selectivity displayed by antitumor spermidine-1,4-NQs and *nor*-lapachol might be an interesting feature if the goal is degradation of amines that are metabolized by both MAO isoforms.

Docking of antitumor 1,4-NQs with MAO isoforms

To understand the structural features associated with the inhibitory properties of lapachol, *nor*-lapachol, and spermidine-1,4-NQs on MAO isoforms, molecular docking studies were carried out. As described in the Experimental section, the Ensemble Docking method, using AutoDock Vina, was carried out taking receptor's structures from snapshots obtained by MD simulations. For docking of all ligands into MAO-A or MAO-B, we have chosen the receptor structures from MD with favorable docking poses that correspond to the snapshots at t = 30 nseconds and t = 20 nseconds for the MAO-A and MAO-B structures, respectively. AutoDock Vina was used as the first approach to evaluate the interaction of antitumor 1,4-NQs with MAO isoforms because this program is much faster than Auto-Dock (28,29). Further, AutoDock was applied in a new docking series for the refinement of the results obtained using Autodock Vina. As discussed in the Experimental section, with the AutoDock program, a whole set of conformations is generated, which are arranged in clusters considering the geometrical similarity and ranked according to the interaction energy. Therefore, in our studies, the results were analyzed taking into account not only enzyme–inhibitor interaction energy, but also the orientation of the 1,4-NQ ring in relation to the FAD moiety, the proximity of the inhibitor to the FAD, and the number of hydrogen bonds (HB) between the ligand and the residues of the active site (Table 3).

The most stable conformations (clusters of most negative interaction energy) generated by docking lapachol or *nor*-lapachol with MAO isoforms are shown in Figure 3.

Table 3: Docking of antitumor 1,4-NQs into active site of MAO isoforms

	MAO-A				MAO-B			
	Energy (kcal/mol)	Orientation 1,4-NQ/FAD	FAD	HB	Energy (kcal/mol)	Orientation 1,4-NQ/FAD	FAD	HB
a_2	−9.44	Perpendicular	HB	3	−8.08	Parallel	Close	No
b_2	−9.85	Parallel	Close	2	−8.15	Parallel	HB	3
c_2	−9.33	Perpendicular	Close	1	−7.32	Parallel	Close	1
Lapachol	−7.08	Perpendicular	Close	No	−7.78	–	Far	2
Nor-lapachol	−7.00	Perpendicular	Close	No	−7.39	Perpendicular	Close	2

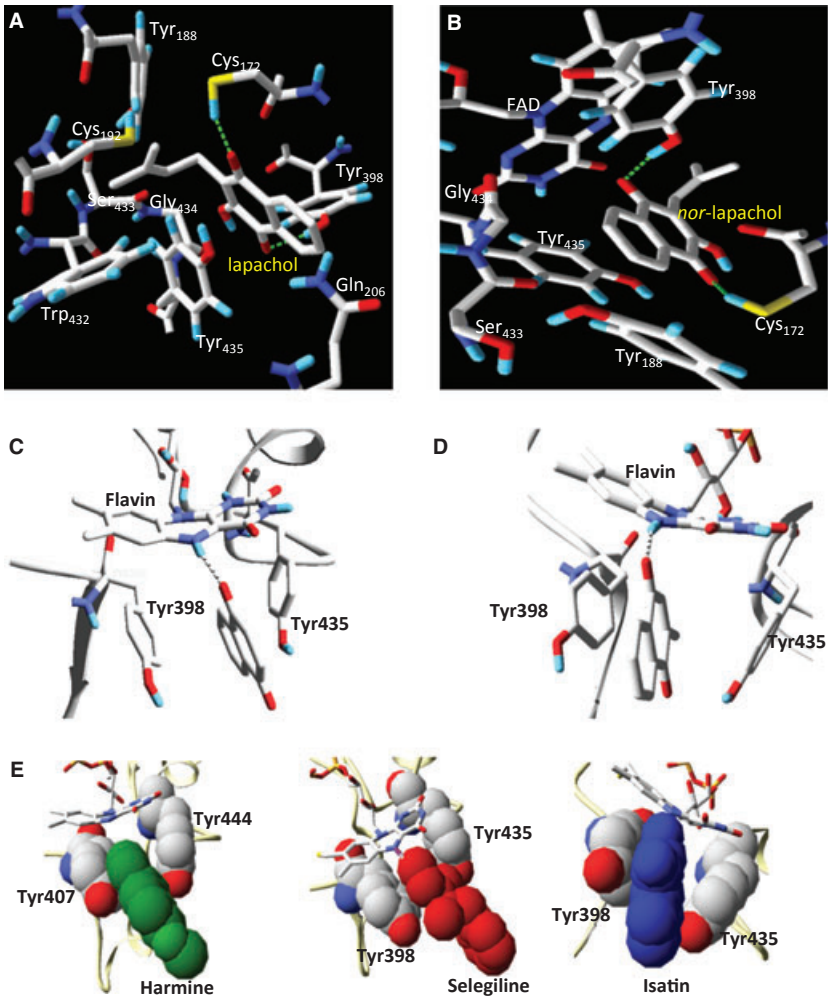

Figure 3: Docking of MAO inhibitors into the active site of MAO isoforms. The MAO-B isoform is shown in the presence of lapachol (A), *nor*-lapachol (B). For comparison, the interaction of 1,4-NQ (C) and menadione (D) with FAD into the MAO-B active site was illustrated; (E) Stabilizing effect due to the formation of an 'aromatic sandwich' between the reversible MAO-A inhibitor harmine with the tyrosine residues Tyr407/444 in MAO-A as well as for the reversible and irreversible MAO-B inhibitors, isatin and selegiline, respectively, with Tyr398/435 in MAO-B. The illustrations were built using the program SwissPDB Viewer 4.0.4.

The kinetic studies have indicated that lapachol is a less potent MAO-B inhibitor than *nor*-lapachol, with *Ki* values of 59 and 18 μM, respectively. The Table 3 shows that the energy of interaction of lapachol or *nor*-lapachol with MAO-B was nearly similar and both inhibitors display two HBs with the residues Cys172 and Tyr398 in the active site of MAO-B (Table S1). However, in the lowest energy conformation, lapachol in MAO-B active site is not close enough to form effective interactions with the flavin moiety, whereas *nor*-lapachol displays interaction with FAD (Figure 3A and B). Moreover, a higher proximity between *nor*-lapachol and the residues Tyr398 and Tyr435 of MAO-B was observed. These differences could explain the greater inhibitory activity of *nor*-lapachol in comparison with lapachol. Our previous studies on the interaction of 1,4-NQ or menadione with MAO-B revealed that the naphthoquinone ring is positioned between Tyr435 and Tyr398 residues in MAO-B, perpendicularly to the re-face of flavin moiety of

FAD cofactor, which allows the phenolic side chains to form an 'aromatic sandwich' structure (Figure 3C and D) (13). Both 1,4-NQ and menadione interact with flavin through a HB. Similar stabilizing effect was described for the reversible MAO-A inhibitor harmine with the tyrosine residues Tyr407/444 in MAO-A, and for the MAO-B inhibitors isatin (reversible) and selegiline (irreversible) with Tyr398/435 in MAO-B (Figure 3E). Crystallographic data suggest that both inhibitors and substrates must pass between these two tyrosines to interact with the flavin group, making this 'aromatic sandwich' an important feature for enzyme functionality (40). Overall, these findings suggest that the close proximity of *nor*-lapachol and the FAD moiety as well as the orientation of the 1,4-NQ ring of the inhibitor and its location into the Tyr435/Tyr398 aromatic sandwich might contribute to the inhibitory properties against MAO-B.

Lapachol did not inhibit significantly MAO-A at a concentration of up to 100 μM, whereas *nor*-lapachol exhibited a *Ki* of 35 μM. The AutoDock results have indicated that the energy of interaction of lapachol or *nor*-lapachol with MAO-B is more favorable (more negative) than observed for MAO-A. In the lowest energy cluster, lapachol and *nor*-lapachol interact with MAO-B with energy of −7.78 and −7.39 kcal/mol, respectively (Table 3). For MAO-A with either lapachol or *nor*-lapachol, the lowest energies of interaction were −7.08 and −7.00 kcal/mol, respectively. Furthermore, lapachol and *nor*-lapachol did not display any HB with the residues in MAO-A active site (Table S1). Although both inhibitors are located close to the FAD moiety of MAO-A and their 1,4-NQ rings are oriented perpendicularly to FAD as observed for *nor*-lapachol with MAO-B, the lower energy of interaction with the absence of HBs might explain the less pronounced inhibitory properties of these molecules against MAO-A.

The analysis of the interaction of MAO-B with **a$_2$**, **b$_2$**, or **c$_2$**, in the lowest energy conformation, indicated that the 1,4-NQ ring is positioned close to the flavin moiety of FAD cofactor in a parallel orientation. In this case, the energies of interaction were −8.08, −8.15, and −7.32 kcal/mol for **a$_2$**, **b$_2$**, and **c$_2$**, respectively. Importantly, **b$_2$** was the only antitumor 1,4-NQ that forms a HB with FAD into the active site of MAO-B. **b$_2$** builds three HBs, with FAD, Leu171, and Tyr398, whereas **c$_2$** only one, with Cys172, and **a$_2$** neither (Table S2). These data might explain the fact of **b$_2$** was the most potent MAO-B inhibitor among the spermidine derivatives with a *Ki* of 12 μM (Table 3).

For MAO-A, the energies of interaction with **a$_2$**, **b$_2$**, and **c$_2$**, in the lowest energy conformation, were −9.44, −9.85, and −9.33 kcal/mol, respectively. In this case, **a$_2$** builds three HBs, with FAD, Gly67, and Gln215 in active site and was the strongest MAO-A inhibitor with a *Ki* of 22 μM. On the other hand, **b$_2$** and **c$_2$** form, respectively, two and one HB with Ile180. Analyzing the **a$_2$** docked in the active site of MAO-A, one can verify that this ligand is positioned in MAO-A differently than observed in MAO-B. For MAO-A, the 1,4-NQ ring is oriented perpendicularly to the flavin ring instead of parallel as found in MAO-B. Moreover, the interaction of **a$_2$** with MAO-A displays more HBs than with MAO-B.

Overall, the docking results suggested that spermidine-1,4-NQs that act as potent inhibitors of MAO are capable of binding to the catalytic cavity of MAO in close proximity of flavin moiety. Furthermore, the formation of HBs between these compounds and FAD and/or the residues in the active site might explain their ability to inhibit both MAO-A and MAO-B. Interestingly, the most potent inhibitors of MAO-A and MAO-B among the spermidine-1,4-NQs, **a$_2$**, and **b$_2$**, respectively, are the only capable of forming HB with the flavin besides a number of HBs with residues in the catalytic site. Considering that **b$_2$** is oriented parallel to the flavin in MAO-B, whereas **a$_2$** is perpendicular to the flavin in MAO-A, we can speculate that the 1,4-NQ ring orientation in relation to the flavin does not play a critical role for MAO inhibition by spermidine-1,4-NQs.

Topoisomerase and MAO as targets for cancer therapy

The inhibition of DNA topoisomerases is an important strategy in cancer therapy due to the role of these enzymes in the modulation of the topological state of DNA and in apoptosis (41). *In vitro* cytotoxic studies of spermidine-1,4-NQs against diverse cancer cell lines demonstrated that these polyamine-conjugates displayed a higher activity than lapachol, *nor*-lapachol or lawsone, according to the activity of these compounds on topoisomerase inhibition. Spermidine-1,4-NQs **a$_2$**, **b$_2$**, and **c$_2$** are capable to induce DNA fragmentation in HL-60 cells at the dose of 25 μM, while only partial inhibition of topoisomerase-2-alpha was observed for lapachol at 200 μM (18). Importantly, no effect of the R-side chain on the activity of the spermidine-1,4-NQs conjugates was observed, in contrast with that verified for the inhibitory activity on MAO. These data suggest that the cytotoxic activity of these compounds on cancer cells, at least in *in vitro* studies, cannot be associated with their inhibitory activity on MAO, even though the action on MAO might influence their antitumoral properties.

Ornithine decarboxylase, an enzyme involved in polyamine biosynthesis, is enhanced in tumor cells, which results in an increase pool of polyamines such as spermine and spermidine that are necessary for cell growth (42). The degradation of these amines by polyamine oxidase and MAO action is accompanied by an elevation of the production of cytotoxic metabolites, such as hydrogen peroxide and aldehydes (43). Therefore, MAO plays an important function not only in the process of cell growth and differentiation but also in the development and growth regulation of tumors. In this context, MAO inhibitors might

interfere in these processes by controlling the formation of hydrogen peroxide and aldehydes from MAO action (43,44).

Conclusions

Spermidine-1,4-NQs, lapachol, and *nor*-lapachol behave as reversible and competitive MAO inhibitors in which the enzyme selectivity and the potency of the inhibitor might be greatly influenced by substitutions on different positions of the 1,4-NQ ring. These data reinforce the idea that 1,4-NQ is a potential pharmacophore for the development of MAO inhibitors and, more importantly, suggest that certain antitumor 1,4-NQs might block MAO activity. Although spermidine-1,4-NQs exhibit antitumor action primarily by inhibiting topoisomerase via DNA intercalation, our findings suggest that their effect on MAO activity should be taken into account when their application in cancer therapy is considered. Whether the inhibitory activity on MAO of spermidine-1,4-NQs, lapachol, and *nor*-lapachol contributes positively or negatively to the tumor growth is a question for further investigations.

Acknowledgments

This work was supported by Souza Cruz Co., Fundação de Amparo à Pesquisa do Estado do Rio de Janeiro (FAPERJ), Conselho Nacional de Desenvolvimento Científico e Tecnológico (CNPq) and International Foundation for Science (IFS). P.A.N and V.P.C are grateful to the National Supercomputing Center – CESUP/UFRGS.

References

1. Youdim M.B., Bakhle Y.S. (2006) Monoamine oxidase: isoforms and inhibitors in Parkinson's disease and depressive illness. Br J Pharmacol;147:287–296.
2. Javitch J.A., D'Amato R.J., Strittmatter S.M., Snyder S.H. (1985) Parkinsonism-inducing neurotoxin, N-methyl-4-phenyl-1,2,3,6 -tetrahydropyridine: uptake of the metabolite N-methyl-4-phenylpyridine by dopamine neurons explains selective toxicity. Proc Nat Acad Sci USA;82:2173–2177.
3. Langston J.W., Langston E.B., Irwin I. (1984) MPTP-induced parkinsonism in human and non-human primates - clinical and experimental aspects. Acta Neurol Scand Suppl;100:49–54.
4. Fowler J.S., Logan J., Volkow N.D., Wang G.J., MacGregor R.R., Ding Y.S. (2002) Monoamine oxidase: radiotracer development and human studies. Methods;27:263–277.
5. Maurel A., Hernandez C., Kunduzova O., Bompart G., Cambon C., Parini A., Francés B. (2003) Age-dependent increase in hydrogen peroxide production by cardiac monoamine oxidase A in rats. Am J Physiol Heart Circ Physiol;284:1460–1467.
6. Marcozzi G., Befani O., Mondovì B. (1998) Type B monoamine oxidase activity in human brain malignant tumors. Cancer Biochem Biophys;16:287–294.
7. Gabilondo A.M., Hostalot C., Garibi J.M., Meana J.J., Callado L.F. (2008) Monoamine oxidase B activity is increased in human gliomas. Neurochem Int;52:230–234.
8. Mondovì B., Riccio P., Riccio A., Marcozzi G. (1983) Amine oxidase activity in malignant human brain tumors. In: Bachrach U., Kaye A., Chayen R., editors. Advances in Polyamine Research 4. New York: Raven Press.
9. Igosheva N., Lorz C., O'Conner E., Glover V., Mehmet H. (2005) Isatin, an endogenous monoamine oxidase inhibitor, triggers a dose- and time-dependent switch from apoptosis to necrosis in human neuroblastoma cells. Neurochem Int;47:216–224.
10. Toninello A., Salvi M., Pietrangeli P., Mondovi B. (2004) Biogenic amines and apoptosis: minireview article. Amino Acids;26:339–343.
11. Zhao H., Flamand V., Peehl D.M. (2009) Anti-oncogenic and pro-differentiation effects of clorgyline, a monoamine oxidase A inhibitor, on high grade prostate cancer cells. BMC Med Genomics;2:55–69.
12. Khalil A.A., Steyn S., Castagnoli N. (2000) Isolation and characterization of a monoamine oxidase inhibitor from tobacco leaves. Chem Res Toxicol;13:31–35.
13. Coelho-Cerqueira E., Netz P.A., Diniz C., Petry do Canto V., Follmer C. (2011) Molecular insights into human monoamine oxidase (MAO) inhibition by 1,4-naphthoquinone: evidences for menadione (vitamin K3) acting as a competitive and reversible inhibitor of MAO. Bioorg Med Chem;19:7416–7424.
14. Balassiano I.T., De Paulo S.A., Henriques Silva N., Cabral M.C., da Gloria da Costa Carvalho M. (2005) Demonstration of the lapachol as a potential drug for reducing cancer metastasis. Oncol Rep;13:329–333.
15. Bermejo-Bescós P., Martín-Aragón S., Jiménez-Aliaga K.L., Ortega A., Molina M.T., Buxaderas E., Orellana G., Csákÿ A.G. (2010) *In vitro* antiamyloidogenic properties of 1,4-naphthoquinones. Biochem Biophys Res Commun;400:169–174.
16. Silva F.L., Coelho-Cerqueira E., Freitas M.S., Gonçalves D.L., Costa L.T., Follmer C. (2013) Vitamins K interact with N-terminus α-synuclein and modulate the protein fibrillization *in vitro*. Exploring the interaction between quinones and α-synuclein. Neurochem Int;62:103–112.
17. Hadden M.K., Hill S.A., Davenport J., Matts R.L., Blagg B.S. (2009) Synthesis and evaluation of Hsp90 inhibitors that contain 1,4-naphthoquinone scaffold. Bioorg Med Chem;17:634–640.
18. Esteves-Souza A., Lucio K.A., Cunha A.S., Cunha Pinto A., Silva Lima E.L., Camara C.A., Vargas M.D., Gattass C.R. (2008) Antitumoral activity of new

polyamine-naphthoquinone conjugates. Oncol Rep;20:225–231.
19. Toninello A., Salvi M., Mondovì B. (2004) Interaction of biologically active amines with mitochondria and their role in the mitochondrial- mediated pathway of apoptosis. Curr Med Chem;11:2349–2374.
20. Agostinelli E., Arancia G.Dalla., Vedova L., Belli F., Marra M., Salvi M., Toninello A. (2004) The biological functions of polyamine oxidation products by amine oxidases: perspectives of clinical applications. Amino Acids;27:347–358.
21. Cunha A.S., Lima E.L.S., Pinto A.C., Esteves-Souza A., Echevarria A., Camara C.C., Vargas M.D., Torres J.C. (2006) Synthesis of novel naphthoquinone-spermidine conjugates and their effect on DNA topoisomerases I and II-α. J Braz Chem Soc;17:439–442.
22. Guang H., Du G. (2006) High-throughput screening for monoamine oxidase-A and monoamine oxidase-B inhibitors using one-step fluorescence assay. Acta Pharmacol Sinica;27:760–766.
23. Dixon M. (1953) The determination of enzyme inhibitor constants. Biochem J;55:170–171.
24. Dennington R., Keith T., Millam J. (2007) GaussView, Version 4.1. Shawnee Mission, KS: Semichem Inc.
25. Frisch M.J., Trucks G.W., Schlegel H.B., Scuseria G.E., Robb M.A., Cheeseman J.R., Scalmani G. *et al.* (2009) Gaussian 09, Revision A.1. Wallingford, CT: Gaussian, Inc.
26. Sanner M.F. (1999) Python: a programming language for software integration and development. J Mol Graph Model;17:57–61.
27. Gasteiger J., Marsili M. (1980) Iterative partial equalization of orbital electronegativity – a rapid access to atomic charges. Tetrahedron;36:3219–3228.
28. Morris G.M., Goodsell D.S., Halliday R.S., Huey R., Hart W.E., Belew R.K., Olson A.J. (1998) Automated docking using Lamarckian Genetic Algorithm and an empirical binding free-energy function. J Comput Chem;19:1639–1662.
29. Huey R., Morris G.M., Olson A.J., Goodsell D.S. (2007) A semiempirical free energy force field with charge-based desolvation. J Comput Chem;28:1145–1152.
30. Trott O., Olson A.J.J. (2010) Auto-DockVina: improving the speed and accuracy of docking with a new scoring function, efficient optimization, and multithreading. Comput Chem;31:455–461.
31. Son S.Y., Ma J., Kondou Y., Yoshimura M., Yamashita E., Tsukihara T. (2008) Structure of human monoamine oxidase A at 2.2-A resolution: the control of opening the entry for substrates/inhibitors. Proc Natl Acad Sci USA;105:5739–5744.
32. Binda C., Wang J., Li M., Hubalek F., Mattevi A., Edmondson D.E. (2008) Structural and mechanistic studies of arylalkylhydrazine inhibition of human monoamine oxidases A and B. Biochemistry;47:5616–5625.
33. Lin J.H., Perryman A.L., Schames J.R., McCammon J.A. (2002) Computational drug design accommodating receptor flexibility: the relaxed complex system. J Am Chem Soc;124:5632–5633.
34. Lin J.H., Perryman A.L., Schames J.R., McCammon J.A. (2003) The relaxed complex method: accommodating receptor flexibility for drug design with and improved scoring scheme. Biopolymers;68:47–62.
35. Sinko W., Lindert S., McCammon J.A. (2013) Accounting for receptor flexibility and enhanced sampling methods in computer-aided drug design. Chem Biol Drug Des;81:41–49.
36. Lindahl E., Hess B., van der Spoel D. (2001) GROMACS 3.0: a package for molecular simulation and trajectory analysis. J Mol Model;7:306–317.
37. Oostenbrink C., Villa A., Mark A.E., van Gunsteren W.F. (2004) A biomolecular force field based on the free enthalpy of hydration and solvation: the GROMOS force-field parameter sets 53A5 and 53A6. J Comput Chem;25:1656–1676.
38. Morris G.M., Huey R., Lindstrom W., Sanner M.F., Belew R.K., Goodsell D.S., Olson A.J. (2009) Autodock4 and AutoDockTools4: automated docking with selective receptor flexibility. J Comput Chem;16:2785–2791.
39. Da Prada M., Zürcher G., Wüthrich I., Haefely W.E. (1988) On tyramine, food, beverages and the reversible MAO inhibitor moclobemide. J Neural Transm Suppl;26:31–56.
40. Nagatsu T., Sawada M. (2006) Molecular mechanism of the relation of monoamine oxidase B and its inhibitors to Parkinson's disease: possible implications of glial cells. J Neural Transm Suppl;71:53–65.
41. Chikamori K., Grozav A.G., Kozuki T., Grabowski D., Ganapathi R., Ganapathi M.K. (2010) DNA topoisomerase II enzymes as molecular targets for cancer chemotherapy. Curr Cancer Drug Targets;10:758–771.
42. Russel D.H. (1980) Ornithine decarboxylase as a biological and pharmacological tool. Pharmacology;20:117–121.
43. Pietrangeli P., Mondovì B. (2004) Amine oxidases and tumors. Neurotoxicology;25:317–324.
44. Maslinski C., Bieganski T., Fogel W.A., Kitler M.A. (1985) Diamine oxidase in developing tissues. In: Mondoví B., editor. Structure and Functions of Amine Oxidases. Boca Raton, FL: CRC Press; p. 153–166.

Supporting Information

Additional Supporting Information may be found in the online version of this article:

Table S1. Interaction of lapachol and *nor*-lapachol with the FAD/residues into active site of MAO in the lowest energy conformation

Table S2. Interactions of anti-tumor spermidine-1,4-NQs with the FAD/residues into active site of MAO isoforms in the lowest energy conformation